

*ARMY RESEARCH LABORATORY*



## **Inductance of Parallel Plates in Electromagnetic Armor**

**by Charles R. Hummer**

**ARL-TR-3788**

**May 2006**

## **NOTICES**

### **Disclaimers**

The findings in this report are not to be construed as an official Department of the Army position unless so designated by other authorized documents.

Citation of manufacturer's or trade names does not constitute an official endorsement or approval of the use thereof.

**DESTRUCTION NOTICE**—Destroy this report when it is no longer needed. Do not return it to the originator.

# **Army Research Laboratory**

Aberdeen Proving Ground, MD 21005-5066

---

**ARL-TR-3788**

**May 2006**

---

## **Inductance of Parallel Plates in Electromagnetic Armor**

**Charles R. Hummer**  
**Weapons and Materials Research Directorate, ARL**

<b>REPORT DOCUMENTATION PAGE</b>			<i>Form Approved</i> <i>OMB No. 0704-0188</i>	
Public reporting burden for this collection of information is estimated to average 1 hour per response, including the time for reviewing instructions, searching existing data sources, gathering and maintaining the data needed, and completing and reviewing the collection information. Send comments regarding this burden estimate or any other aspect of this collection of information, including suggestions for reducing the burden, to Department of Defense, Washington Headquarters Services, Directorate for Information Operations and Reports (0704-0188), 1215 Jefferson Davis Highway, Suite 1204, Arlington, VA 22202-4302. Respondents should be aware that notwithstanding any other provision of law, no person shall be subject to any penalty for failing to comply with a collection of information if it does not display a currently valid OMB control number. <b>PLEASE DO NOT RETURN YOUR FORM TO THE ABOVE ADDRESS.</b>				
<b>1. REPORT DATE (DD-MM-YYYY)</b> May 2006		<b>2. REPORT TYPE</b> Final		<b>3. DATES COVERED (From - To)</b> May 2004 to December 2004
<b>4. TITLE AND SUBTITLE</b>  Inductance of Parallel Plates in Electromagnetic Armor			<b>5a. CONTRACT NUMBER</b>	
			<b>5b. GRANT NUMBER</b>	
			<b>5c. PROGRAM ELEMENT NUMBER</b>	
<b>6. AUTHOR(S)</b>  Charles R. Hummer (ARL)			<b>5d. PROJECT NUMBER</b> 622105.AH84	
			<b>5e. TASK NUMBER</b>	
			<b>5f. WORK UNIT NUMBER</b>	
<b>7. PERFORMING ORGANIZATION NAME(S) AND ADDRESS(ES)</b> U.S. Army Research Laboratory Weapons and Materials Research Directorate Aberdeen Proving Ground, MD 21005-5069			<b>8. PERFORMING ORGANIZATION REPORT NUMBER</b>  ARL-TR-3788	
<b>9. SPONSORING/MONITORING AGENCY NAME(S) AND ADDRESS(ES)</b>			<b>10. SPONSOR/MONITOR'S ACRONYM(S)</b>	
			<b>11. SPONSOR/MONITOR'S REPORT NUMBER(S)</b>	
<b>12. DISTRIBUTION/AVAILABILITY STATEMENT</b>  Approved for public release; distribution is unlimited.				
<b>13. SUPPLEMENTARY NOTES</b>				
<b>14. ABSTRACT</b>  In electromagnetic armor, a shaped charge jet is disrupted when a large current is passed through it while the jet is in contact with two parallel flat plates. For the current to increase as quickly as possible to an effective level, the inductance of the circuit must be controlled or at least known. This inductance, however, depends on the position of the current connections to the plates and the position of the shaped charge jet. A method to calculate this inductance is presented, which is verified by experimental measurements.				
<b>15. SUBJECT TERMS</b> inductance; magnetic field				
<b>16. SECURITY CLASSIFICATION OF:</b>			<b>17. LIMITATION OF ABSTRACT</b>  SAR	<b>18. NUMBER OF PAGES</b>  35
<b>a. REPORT</b> Unclassified	<b>b. ABSTRACT</b> Unclassified	<b>c. THIS PAGE</b> Unclassified		
			<b>19b. TELEPHONE NUMBER (Include area code)</b> 410-278-5680	

---

## Contents

---

<b>List of Figures</b>	<b>iv</b>
<b>List of Tables</b>	<b>iv</b>
<b>1. Description of Technology</b>	<b>1</b>
<b>2. Experimental Arrangement</b>	<b>1</b>
<b>3. Current Distribution</b>	<b>3</b>
<b>4. Plate Inductances</b>	<b>13</b>
<b>5. Conclusion</b>	<b>16</b>
<b>6. References</b>	<b>17</b>
<b>Appendix A. Integrals for the Inductance Calculation</b>	<b>19</b>
<b>Distribution List</b>	<b>29</b>

---

## List of Figures

---

Figure 1. Experimental arrangement.....	2
Figure 2. Current distribution in a thin plate.....	4
Figure 3. Right cylinder with an arbitrary cross section carrying a current. ....	5
Figure 4. Magnetic field lines of a flat ribbon carrying a uniform current.....	6
Figure 5. Magnetic field lines of a flat ribbon with a current distribution given by equation 7....	8
Figure 6. Current distribution of a small rectangle on the plate. ....	10
Figure 7. Inductance of two parallel plates for hit locations along the mid line.....	13
Figure 8. Convergence as a function of the inverse number of grid points.....	15

---

## List of Tables

---

Table 1. 1.0 cm by 0.5 cm.....	14
Table 2. 1.0 cm by 1.0 cm.....	14
Table 3. 1.0 cm by 2.0 cm.....	15

---

## 1. Description of Technology

---

A shaped charge jet is formed by the detonation of a high explosive that surrounds the outside of a hollow right circular cone of copper. As the detonation front in the high explosive travels from the vertex to the base of the cone, the copper is propelled toward the central axis of the cone. The flow of copper toward the central axis results in the formation of a thin jet of copper (shaped charge jet) traveling at a high velocity along the central axis and directed outward through the base of the cone. This non-molten shaped charge jet is capable of penetrating thick armor.

It was proposed (1) that a large electric current flowing along the shaped charge jet could vaporize the jet and make it harmless. In this proposal, the electric current was applied to the jet by two thin metal plates that are parallel with each other and separated by some distance. A conductive path from one metal plate to the other is formed after the jet penetrates each metal plate. A current source that is connected to the plates can now apply a current along the jet. At the time of the proposal, however, a magnetic flux compressor was the only type of current source that could generate a large enough current in the time needed to vaporize the jet. Since then, it has been shown that an electric current can enhance the inherent hydrodynamic instabilities in the jet and cause the jet to break into a string of particles that cannot penetrate as much armor as a continuous jet (2). It has also been shown that a jet heated (by an electric current) to a point where it melts will break and expand into a series of rings that have little penetration into armor (3). The current needed to drive the hydrodynamic instabilities or to melt the jet is far less than the current needed to vaporize the jet. Because less current is needed to reduce the penetration of the jet into armor, it is possible to use a capacitor bank as a current source. Indeed, capacitor banks have become the current source for many experiments in electro-magnetic armor (EMA) (4).

---

## 2. Experimental Arrangement

---

The experimental arrangement for many EMA experiments is illustrated in figure 1. The parallel plates are connected to a remotely located capacitor bank C by the way of coaxial cables, strip line, or a transmission line of some design. Also shown in figure 1 is an illustration of a shaped charge jet traveling downward and positioned just when the tip of jet, point A, contacts the bottom plate and completes a conducting path. At this time, the current starts to flow from the capacitor bank and through the jet. For a time after the initial contact, the current increases at a steady rate, starting from zero current. Because the tip of the jet perforates the bottom plate almost immediately after the current starts, the current has little time to increase to an effective level, and there is little time to drive the hydrodynamic instabilities near the tip or to melt the tip.

In contrast, EMA affects the portion of the jet farther back from the tip such as the portion near point B in figure 1. During the time that point B travels to the bottom plate, there is time for the current to increase to an effective level, and there is time to drive the hydrodynamic instabilities or melt the jet. Thus the rate at which the current increases after the initial contact must be as large as possible so that the length of the jet after the tip that is not affected by the current is reduced.

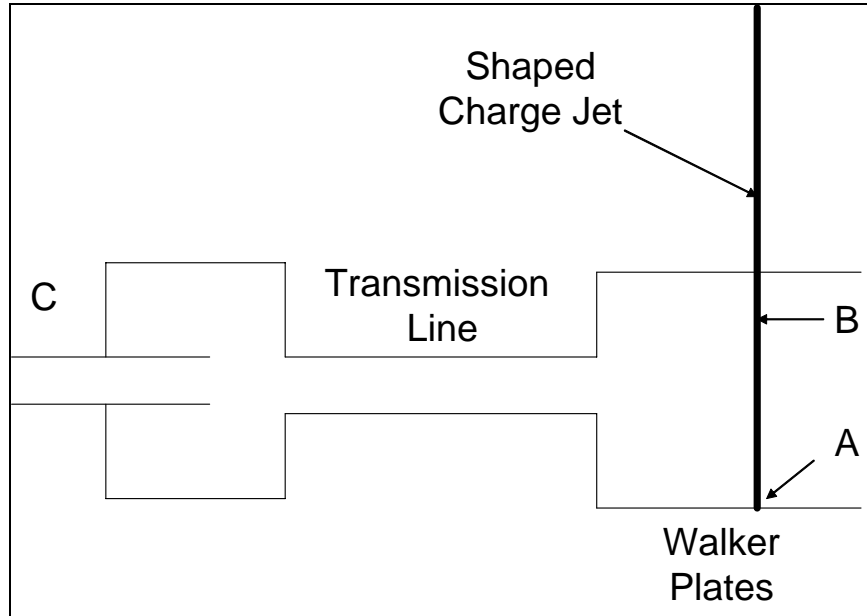


Figure 1. Experimental arrangement.

The initial rate of the current just after the initial contact  $dI_0/dt$  for the circuit in figure 1 is given by  $dI_0/dt = V/L_t$ , in which  $V$  is the initial voltage on the capacitor bank and  $L_t$  is the total inductance of the circuit. A large  $dI_0/dt$  would result by a large  $V$  and a small  $L_t$ . In this circuit, the total inductance  $L_t$  includes the inductance in the capacitors, the connections to the plates, the plates, and the shaped charge jet. As a typical example (4), if the initial voltage on the capacitor bank is 10 kV and if the  $dI_0/dt$  is to be 20 kA/ $\mu$ s,  $L_t$  would then be 0.5  $\mu$ H. It is possible to design the capacitors and the connections to the plates so that their inductances are a small contribution to the total inductance. The inductance of the parallel plates could be made small if their separation distance were small. A small separation distance, however, reduces the effectiveness of the armor because the time that a portion of the jet is between the plates and being acted upon by the current is small. This reduction in the effectiveness of the armor can be compensated by a larger current. In contrast, if the separation distance is increased, the times that portions of the jet are between the plates and being acted upon by the current increase, which results in less current to destroy the jet. Larger separation distances, however, would increase the total inductance of the circuit resulting in an increase of the time for the current buildup to become effective. During this buildup time of the current, a portion of the jet near the tip is passing intact through the bottom plate in figure 1. This buildup time for the current can be



decreased if a larger charge voltage is used on the capacitor bank. Thus, the plate design depends on the power supply and the characteristics of the shaped charge jet.

To design an EMA system, the first step is to identify a shaped charge jet to be defeated and then calculate the current and the time required to destroy the various sections of the jet. The next step is to design a pulse power system that will deliver the current in the required time, given the requirements for the specific application of the EMA. The requirements to be addressed here are the protection area and the thickness of the EMA. Suppose that the area and the thickness of EMA are given for some application. Is it better to cover the area with just one set of parallel plates, or is it better to divide the area into a number of parallel plates, each being connected to the capacitor bank by a low inductance transmission line? Considering the inductance of the parallel plates in these two cases and the other requirements of the application may answer the question. Therefore, a method was developed and presented here to calculate the inductance. Because this method is unfortunately rather long and difficult, the results of the calculations are presented in tables 1 through 3 for various plate parameters that are likely to be found in EMA. With these tables, which are presented in section 4, it is possible to quickly estimate the inductance of a wide variety of parallel plates and then change the design for an EMA. Once the design of the EMA has been narrowed, the inductance of the plate could be calculated to further refine the design.

---

### 3. Current Distribution

---

Consider a thin rectangular plate that has a current distribution as shown in figure 2. The lines radiating from the point on the edge represent a point current source on the edge. The place where the lines converge to a point represents a current “sink”. Each line is a flow line where the current density vector is tangential to the line. In EMA, the source on the edge of the plate would be where the plate is connected to the capacitor bank, and the sink would be where the shaped charge jet has penetrated the plate. The current distribution on the opposite parallel plate is similar: a current sink on the edge of the plate where it is connected to the return to the capacitor bank, and a current source where the shaped charge jet has penetrated it. The current distributions in both of the plates are a source of a magnetic field that required some energy to create. This energy  $W_m$  is related to the inductance of the plates by  $W_m = L_p I^2 / 2$ , in which  $L_p$  is the inductance of the plates and  $I$  is the current in the circuit.

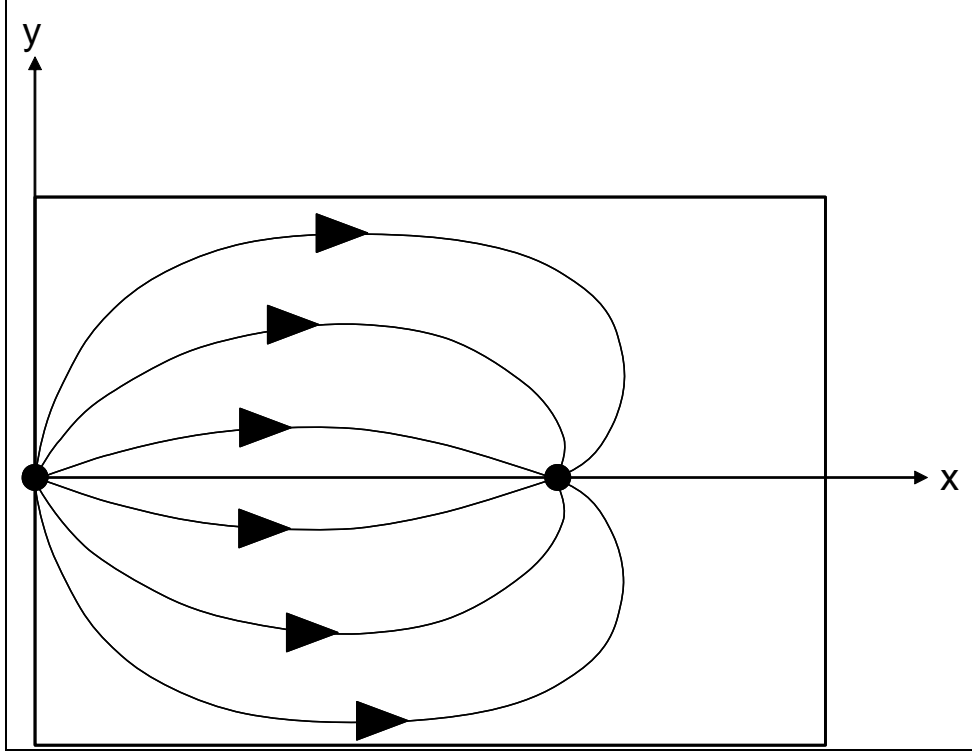


Figure 2. Current distribution in a thin plate.

Since different current distributions in the plates will produce different magnetic fields with different energies, the inductance of the plates will differ. This means that the current distribution of the plates must be known before the inductance of the plates can be calculated. Unfortunately, the current distributions in the plates can be calculated only after some assumptions are made. Each assumption, however, results in a different current distribution and a different plate inductance. Furthermore, none of these assumptions may seem at first to be applicable to EMA. Therefore, these various assumptions are presented here and discussed before we continue to the calculation of the plate inductance.

This discussion serves as a tutorial for how to calculate the energy stored in a magnetic field. The consequences of using these assumptions are illustrated by a common problem that can be solved analytically for most cases. To start, consider a problem as shown in figure 3 that shows a right cylinder with some arbitrary cross section oriented to be parallel with the z-axis. The ends of the right cylinder lie on the  $z = l/2$  plane and the  $z = -l/2$  plane in which  $l$  is the total length of the right cylinder. For all points in the cross section, there is a current density vector  $J_z(x,y)$ , parallel to the z-axis and dependent only on its position on the x-y plane. Now apply the general integral for the energy stored in the magnetic field which is

$$W_m = \frac{1}{2} \int dx^3 \vec{J}(\vec{x}) \cdot \vec{A}(\vec{x}) \quad , \quad (1)$$

where the magnetic vector potential  $\vec{A}(\vec{x})$  is produced by the same current density distribution according to

$$\vec{A}(\vec{x}) = \frac{\mu_o}{4\pi} \int (dx')^3 \frac{\vec{J}(\vec{x}')}{\sqrt{(x-x')^2 + (y-y')^2 + (z-z')^2}} . \quad (2)$$

This integral is taken over the same entire volume as equation 1.

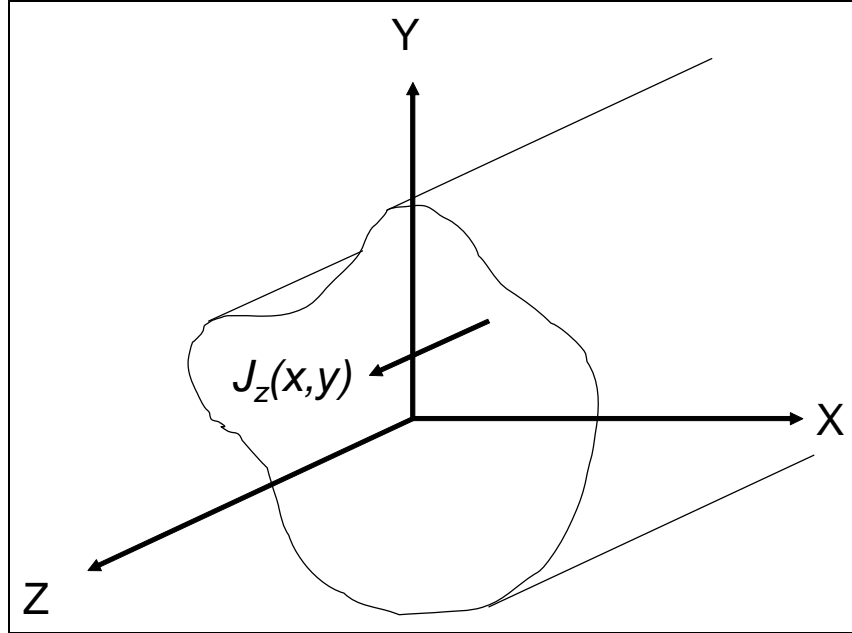


Figure 3. Right cylinder with an arbitrary cross section carrying a current.

When the length of the right cylinder  $l$  is much larger than the maximum length across the cross section and when the current density is independent of the  $z$ -coordinate, equation 1 can be integrated over  $z$  and  $z'$  to become

$$W_m = \frac{\mu_o l}{4\pi} \int dx dy dx' dy' J_z(x, y) J_z(x', y') \ln \left( \frac{2l}{\sqrt{(x-x')^2 + (y-y')^2}} \right) . \quad (3)$$

With the properties of the logarithm, this integral may also be written as

$$W_m = \frac{\mu_o l \ln(2l) I^2}{4\pi} - \frac{\mu_o l}{8\pi} \int dx dy dx' dy' J_z(x, y) J_z(x', y') \ln \left( (x-x')^2 + (y-y')^2 \right) , \quad (4)$$

in which  $I$  is the total current in the conductor. Now apply equation 4 to a flat ribbon with a width  $w$  that is located on the  $x$ -axis as shown in figure 4 which gives

$$W_m = \frac{\mu_o l \ln(2l) I^2}{4\pi} - \frac{\mu_o l}{4\pi} \int dx dx' J_z(x) J_z(x') \ln(|x-x'|) . \quad (5)$$

Now an assumption must be made that will result in a current distribution  $J_z(x)$  across the width of the ribbon.

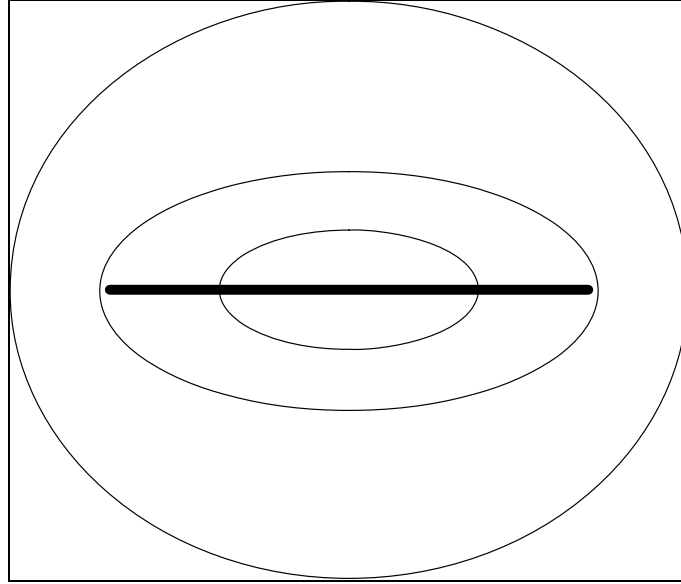


Figure 4. Magnetic field lines of a flat ribbon carrying a uniform current.

The simplest assumption is to have a uniform current density across the ribbon  $J_z(x) = I/w$ , which will result when the current is constant with time and when the ribbon is made of a material with a resistance. After the double integral is performed, the energy stored in the magnetic field for a direct current  $W_m^{d.c.}$  is

$$W_m^{d.c.} = \frac{\mu_o l \ln(2l) I^2}{4\pi} - \frac{\mu_o l I^2}{4\pi} (\ln(w) - 1.5) . \quad (6)$$

The next assumption is to have the ribbon made from a material that has no resistance or a super conductor which changes the boundary conditions of the magnetic field on the ribbon. In this case, the magnetic field inside a super conductor must be zero, which is different from the boundary conditions for an ordinary conductor. On the surface of an ordinary conductor, the normal component of the magnetic induction field  $B$  must be continuous when we are going across the surface. This condition also holds for a super conductor because it is based on the fact that there are no magnetic monopoles. Since  $B$  must be zero inside the super conductor, the normal component of  $B$  on the surface of the super conductor must also be zero. Therefore, the magnetic induction field must be tangential to the surface of the super conductor. For normal conductors, the tangential component of the magnetic field  $H$  must be continuous when crossing the surface, provided that there are no surface currents. For super conductors, however, there are surface currents that can produce a discontinuity of the tangential component of  $H$ . The consequence of these boundary conditions in two-dimensional geometry is that the surface of a super conductor is a field line of the magnetic induction field. To illustrate the differences between a normal conductor and a super conductor, figure 4 shows the magnetic induction field of the ribbon with a uniform current, and figure 5 shows the magnetic induction field when the

ribbon is a super conductor. For a uniform current in figure 4, some of the field lines cross the ribbon, which would not be allowed if the ribbon were a super conductor. The field lines in figure 5 were calculated from a current distribution that excludes all the field lines from the ribbon. From other calculations, it was discovered that this current distribution is

$$J_z(x) = \frac{I}{\pi\sqrt{(w/2)^2 - x^2}} , \quad (7)$$

which becomes infinite at the edges of the ribbon. Substituting this current distribution into equation 3 gives the energy stored in the magnetic field for a super conductor  $W_m^{s.c.}$  to be

$$W_m^{s.c.} = \frac{\mu_o l \ln(2l) I^2}{4\pi} - \frac{\mu_o l I^2}{4\pi} (\ln(w) - \ln(4)) . \quad (8)$$

Since  $\ln(4)$  is 1.386..., the energy stored in the magnetic field for a ribbon carrying a direct current (equation 4) is close to that of a super conducting ribbon with the same width and length and carrying equal current (equation 6). This is in spite of the very different current distributions in the two ribbons.

Finally, it could be assumed that there is an alternating voltage source connected at the ends of the long ribbon and operating at an angular frequency  $\omega$ . The equation to be solved for the current distribution across the ribbon does not have an analytic expression, and it is necessary to use numerical methods to solve the problem. The results of the numerical analysis show that the energy stored in the magnetic field approaches the value given by equation 6 as the angular frequency approaches zero. The analysis also shows that the magnetic energy approaches the value given by equation 8 as the angular frequency approaches infinity. This is the result of the fact that alternating currents in a conductor tend to become more concentrated toward the surface as the angular frequency of the currents increases. At very high frequencies, the currents are concentrated very close to the surface in the same manner as a super conductor. Thus, the assumption that the conductor is a super conductor gives the high frequency limit. The numerical analysis also shows that the magnetic energy for the intermediate angular frequencies is always between  $W_m^{s.c.}$ , the lower limit, and  $W_m^{d.c.}$ , the upper limit.

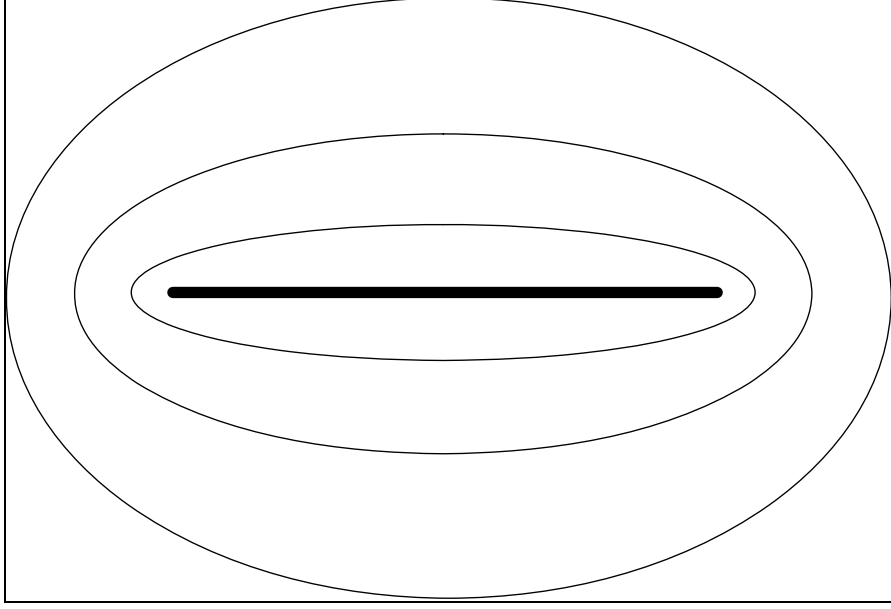


Figure 5. Magnetic field lines of a flat ribbon with a current distribution given by equation 7.

In reviewing all of the previous assumptions, we see that none of them apply directly to EMA where the current is a transient or a pulse: it is not a direct current and it does not have a constant angular frequency. Furthermore, the conductors in EMA are not super conductors. It would seem that none of these assumptions could be applied to EMA to find the magnetic energy stored in the plates and then assign an inductance for them. The examination of the flat ribbon, however, indicates that the magnetic energy is not very sensitive to the exact current distribution in the ribbon. If this observation holds true for the plates in EMA, it is possible to find a good estimate of the inductance of the plates, even though the assumption being used may not be valid and the current distribution in the plates may not be valid. Therefore, it will now be assumed that the current distribution in the EMA plates will be for direct currents. The reason for this choice is because the current distribution for a direct current is easily found with the use of any one of a number of techniques. Whatever technique is used, the current density is no longer an analytic expression and the integration of equations 1 and 2 must be done numerically.

Performing the integrals in equations 1 and 2 numerically requires effort. As an example, suppose that the overall volume is a cube that is subdivided into  $n^3$  smaller cubes, where  $n$  is the number of smaller cubes along each edge of the larger cube. If the magnetic vector potential is to be estimated at a corner of a smaller cube at  $(x,y,z)$ , the integrand in equation 2 must be evaluated at all the  $(n+1)^3$  corners  $(x',y',z')$  of the smaller cubes and summed. This magnetic vector potential is then multiplied with the current density to become a value for the integrand in equation 5 at this corner. This procedure must be repeated for each corner of the smaller cubes at  $(x,y,z)$ . This means that the total number of times that the integrand in equation 2 must be evaluated to find the magnetic energy is on the order of  $(n+1)^6$ . If the cube is divided into 100 smaller cubes per edge, then the total number of evaluations of the integrand is about  $10^{12}$  which

is practical on most computers. If the cube is divided into 1000 smaller cubes per edge, then the total number of evaluations of the integrand is now about  $10^{18}$ , which is not practical even on a super computer. This demonstrates that as the number of points or the number of cubes is increased to capture the finer details of the current distribution in the volume, the labor to find the magnetic energy will dramatically increase. Because the magnetic vector potential and the current density distribution are known after we solve a problem, however, a single integration over the volume, equation 1, is needed to calculate the energy of the magnetic field. Finding the magnetic energy for two infinitely thin plates, each with a current distribution, is easier. Let the two plates be squares, as an example, and divide each plate into  $n^2$ , where  $n$  is the number of squares along each side of the plate. The number of times that the integrand in equation 2 is to be evaluated is now about  $(n+1)^4$  rather than about  $(n+1)^6$ . This is the consequence of the fact that equations 1 and 2 are now integrals over the areas of the thin plates rather than integrals over volumes. Still, a method was used here to estimate the magnetic energy for a very large number of squares from the results using a more practical number of squares.

The result of using the procedures based on finite differences, such as the relaxation method, is an estimate of the current densities at points on a regular rectangular grid on the plate. The plate is now divided into smaller rectangular regions where the current densities are given at each corner. One of these small rectangular regions is shown in figure 6 as an example. The origin of the coordinate frame for the rectangle is placed in the middle and oriented with the x-axis parallel to one side and the y-axis parallel to another side. The rectangle has a half-length “a” and a half-height “b”. The x components of the current densities at the four corners are  $J_x^{-,-}$ ,  $J_x^{+,-}$ ,  $J_x^{+,+}$ , and  $J_x^{-,+}$ . The y components of the current densities at the four corners are  $J_y^{-,-}$ ,  $J_y^{+,-}$ ,  $J_y^{+,+}$ , and  $J_y^{-,+}$ . The signs in superscript give the sign of the x and y directions, respectively, from the origin to the corner. In order to find the magnetic vector potential produced by the current density distribution in this rectangle, the current density must be given at all points on the rectangle, but the current densities are known only at the corners. Therefore, it is necessary to assume a continuous current distribution that is specified by the current densities at the corners. Since there are four given x components of the current density, simply assume that

$$J'_x(x', y') = \alpha'_x + \beta'_x x' + \gamma'_x y' + \delta'_x x' y' \quad , \quad (9)$$

where the coefficients  $\alpha'_x$ ,  $\beta'_x$ ,  $\gamma'_x$ , and  $\delta'_x$  are chosen so that  $J'_x(a, b) = J_x^{+,+}$ ,  $J'_x(-a, b) = J_x^{-,+}$ ,  $J'_x(a, -b) = J_x^{+,-}$ , and  $J'_x(-a, -b) = J_x^{-,-}$ .

In the same manner, assume that

$$J'_y(x', y') = \alpha'_y + \beta'_y x' + \gamma'_y y' + \delta'_y x' y' \quad , \quad (10)$$

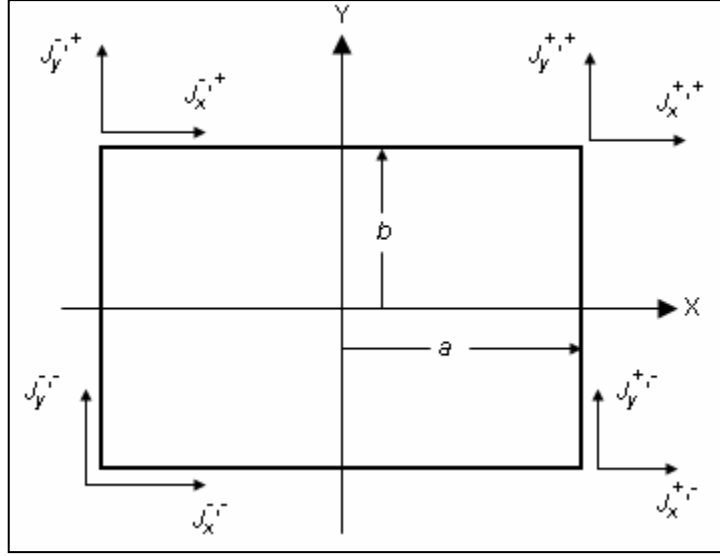


Figure 6. Current distribution of a small rectangle on the plate.

where the coefficients  $\alpha'_y$ ,  $\beta'_y$ ,  $\gamma'_y$ , and  $\delta_y$  are chosen so that  $J'_y(a, b) = J_y^{+,+}$ ,  $J'_y(-a, b) = J_y^{-,+}$ ,  $J'_y(a, -b) = J_y^{+,-}$ , and  $J'_y(-a, -b) = J_y^{-,-}$ . With these assumptions for the neighboring rectangles on the plate, it can be shown that the current density vector is continuous in value as one crosses the edge from one rectangle into a neighboring rectangle. The partial derivatives of the current density vector, however, are not continuous when we cross an edge. In addition, charge may not be conserved within a rectangle, but it could be conserved if  $\delta_x = 0$ ,  $\delta_y = 0$ , and  $\beta_x + \gamma_y = 0$  so that  $\bar{\nabla} \cdot \bar{J} = 0$  everywhere. In spite of these limitations of the assumed current distribution, it is a good approximation of current distributions that do conserve the charge everywhere, provided that the rectangle is small enough so that the conditions for its charge conservation are approximately satisfied. The x-component of the magnetic vector potential for this current distribution is

$$A_x(x, y, z) = \frac{\mu_0}{4\pi} \int_{-a}^a dx' \int_{-b}^b dy' \frac{\alpha'_x + \beta'_x x' + \gamma'_x y' + \delta'_x x' y'}{\sqrt{(x-x')^2 + (y-y')^2 + z^2}} \quad (11)$$

and the y-component of the magnetic vector potential is

$$A_y(x, y, z) = \frac{\mu_0}{4\pi} \int_{-a}^a dx' \int_{-b}^b dy' \frac{\alpha'_y + \beta'_y x' + \gamma'_y y' + \delta'_y x' y'}{\sqrt{(x-x')^2 + (y-y')^2 + z^2}} \quad (12)$$

Both of these sets of integrals have the same form, and they have an analytic expression which is given in appendix A. This rectangle is a source of a magnetic field within which any current distribution will result in an energy as stated by equation 1. The current distribution in just one of the other rectangles on the plate will result in only a part of the total energy for the entire plate. Let the current distribution in the other rectangle be



$$J_x(x, y) = \alpha_x + \beta_x x + \gamma_x y + \delta_x xy \quad , \quad (13)$$

and

$$J_y(x, y) = \alpha_y + \beta_y x + \gamma_y y + \delta_y xy \quad . \quad (14)$$

The energy for these two rectangles is then

$$w_{sf} = \frac{\mu_o}{8\pi} \int_{x_o-c}^{x_o+c} dx \int_{y_o-d}^{y_o+d} dy A_x(x, y, z)(\alpha_x + \beta_x x + \gamma_x y + \delta_x xy) \\ + \frac{\mu_o}{8\pi} \int_{x_o-c}^{x_o+c} dx \int_{y_o-d}^{y_o+d} dy A_y(x, y, z)(\alpha_y + \beta_y x + \gamma_y y + \delta_y xy) \quad , \quad (15)$$

in which  $c$  is the half length and  $d$  is the half height of the other rectangle. It is understood that the two rectangles lie on parallel planes that are separated by the distance  $z$ , and the center of the other rectangle is located at  $(x_o, y_o, z)$ . It is also understood that the sides of one rectangle are parallel or perpendicular to the sides of the other. These integrals are analytic, but their expression, also shown in appendix A, are long and complicated. This expression is applied to all possible pairs of rectangles on the plates and collected as a sum for the total energy. This pairing means that any two given rectangles will be paired together twice: the first rectangle as a source is paired to the second as the one being in the magnetic field of the first, and then the second rectangle as a source is paired to the first as the one being in the magnetic field of the second. Fortunately, the expression needs to be evaluated just once for a given pair of rectangles because it will give the same answer when the two rectangles are interchanged. Once the expression is evaluated for a pair of rectangles, the result is doubled and then added to the total. This pairing includes each rectangle being paired with itself, since each rectangle has a current distribution within a magnetic field of its own creation. Here, the expression is evaluated and added to the total without doubling, since there is only one pairing of a rectangle with itself. This pairing can be divided into three groups. The first group has pairs of rectangles on one plate. The total energy found for this pairing does not change as the distance between the plates change. The second group has pairs of rectangles on the opposing plate. The total energy for this second group is the same as the first. The third group has one rectangle on each separate plate. The total energy from this third group does change with the distance between the plates. Once the total energy,  $W$ , is found, the inductance of the plates is then calculated by  $Lp = 2.0 W/I^2$ , in which  $I$  is the current flowing through the jet.

The explicit expression for the integral in equation 15 becomes numerically unstable when the distance between the two rectangles becomes large. The reason for this instability is that many of the functions used in the expression increase to large values as the distance between the rectangles increases. The integral, however, requires these functions to be subtracted. Subtracting two very large numbers that are nearly equal is a well-known source for round-off

error. At these large distances, it is better and faster to numerically integrate equation 15. Since the magnetic vector potential smoothly varies over the field rectangle at these separation distances, the numerical integration quickly converges. As the separation distance is increased even more, the explicit expression for the magnetic vector also begins to suffer from round-off error. At these distances, it is possible to use a multipole expansion for the magnetic vector potential that is stable for even larger distances, but this was not needed for these calculations.

To validate these calculations, two 29-cm by 68.5-cm plates were mounted in parallel by 10.0-cm-long spacers that were insulators. The plates were 0.6 cm thick. One lead to an inductance meter was attached at the mid point of the 29-cm-long edge of a plate. The other lead to the inductance meter was attached to the other plate directly opposite the first lead. Holes were drilled through the plates at various locations. These holes allowed for a brass rod, 0.63 cm in diameter, to be inserted perpendicularly through each plate and fastened to make contact with each plate. The inductance was measured for a given location of the brass rod, and then the brass rod was moved to another location for another measurement. These measurements would have included the inductance of the plates and the inductance of the brass rod, but the inductance meter was adjusted to subtract the inductance of the brass rod.

To compare the calculated inductance with the measured inductance, we chose the point where the inductance meter is attached as the origin of a coordinate system, as shown in figure 2, where the x-axis is perpendicular to the edge of the plate so that the x-axis runs along the line midway between the two 68.5-cm-long edges of the plate and where the y-axis is parallel to the 29-cm-long edge of the plate. Figure 7 compares the calculated inductance (the smooth solid lines) with the measured inductance (the squares) for rod locations along the x-axis or along the mid-line of the plates. The results of two calculations are shown in figure 7. One calculation assumes that the plates are spaced by 10.0 cm, but the plates have a thickness of 0.6 cm. As a test for the effects of the plate spacing, another calculation was done for a plate spacing of 11.2 cm which is the inside spacing of the plates plus the thickness of both plates. The comparison shows that the calculations can give a good estimate of the plate inductances. In addition, the calculations and the experimental measurements are in similar agreement when the rod was placed at other locations away from the x-axis.

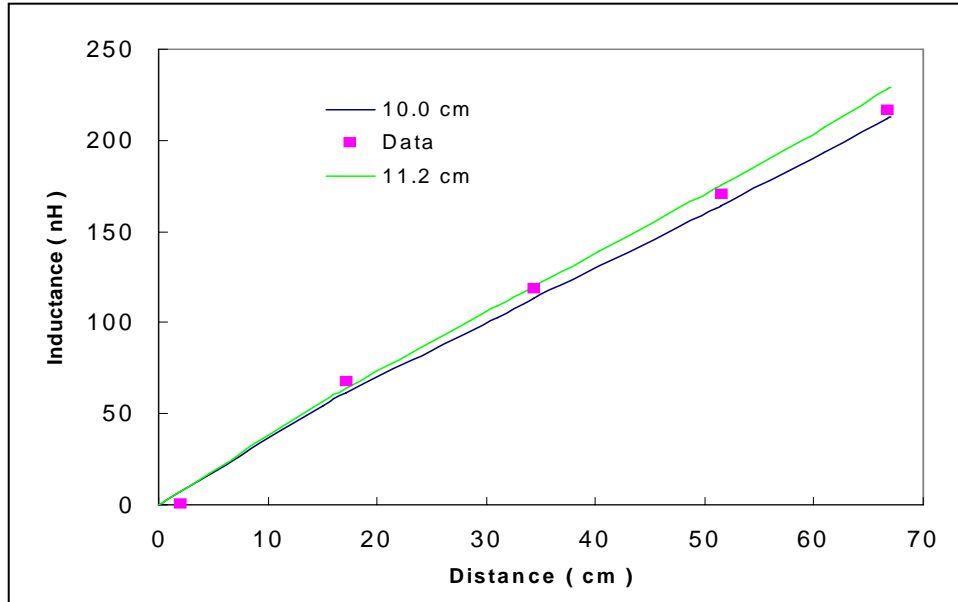


Figure 7. Inductance of two parallel plates for hit locations along the mid line.

---

#### 4. Plate Inductances

---

The inductance of the plates with different aspect ratios, different spacings, and various hit locations was calculated and presented in tables 1 through 3. The procedure for these calculations started with choosing the aspect ratio of the sides of the plates. Next, the location where the current is feeding the plate and the location of the sink or hit were chosen. The current distribution was calculated by a relaxation method after the size of the grid was chosen. Because this current distribution does not change as the spacing between the plates is changed, this current distribution is used in the calculation of the inductance for a number of spacings between the plates. Keeping the locations of the current feed and the sink fixed, the current distribution was found on a finer grid and the inductance was again calculated for the same set of spacings. This procedure was repeated for a number of finer grids. It was observed that the inductance for a given spacing depended on the number of grid points  $n$  along an edge of the plate as  $L(n) = L_0 + a/n + b/n^2$ . An example of the inductance converging to a value is shown in figure 8 where the plate is a 1-cm by 1-cm square with a spacing of 0.1 cm. The current feeds are at the mid points of two opposing edges and the sink is in the center of the square. In this example, the inductance is taken to be the extrapolated value at zero for an inductance of 1.68 nH. All the inductances in tables 1 through 3 resulted in this extrapolation to zero.

Table 1. 1.0 cm by 0.5 cm.

$z = 0.1$	$x = 0.00$	$x = 0.25$	$x = 0.50$
$y = 0.50$	2.111	1.657	2.251
$y = 0.25$	1.168	1.041	1.521
$y = 0.00$	0.000	0.781	1.345
$z = 0.2$	$x = 0.00$	$x = 0.25$	$x = 0.50$
$y = 0.50$	2.926	2.387	3.221
$y = 0.25$	1.523	1.428	2.177
$y = 0.00$	0.000	1.012	1.896
$z = 0.3$	$x = 0.00$	$x = 0.25$	$x = 0.50$
$y = 0.50$	3.388	2.832	3.821
$y = 0.25$	1.696	1.643	2.579
$y = 0.00$	0.000	1.129	2.227
$z = 0.4$	$x = 0.00$	$x = 0.25$	$x = 0.50$
$y = 0.50$	3.681	3.130	4.231
$y = 0.25$	1.795	1.779	2.851
$y = 0.00$	0.000	1.199	2.449
$z = 0.5$	$x = 0.00$	$x = 0.25$	$x = 0.50$
$y = 0.50$	3.881	3.342	4.529
$y = 0.25$	1.857	1.871	3.046
$y = 0.00$	0.000	1.246	2.608

Table 2. 1.0 cm by 1.0 cm.

$z = 0.1$	$x = 0.00$	$x = 0.25$	$x = 0.50$	$x = 0.75$	$x = 1.00$
$y = 0.50$	2.0480	1.5492	1.6800	1.9744	2.5644
$y = 0.25$	1.1396	0.9966	1.2400	1.5302	1.9800
$y = 0.00$	0.0000	0.7280	1.0860	1.3960	1.8618
$z = 0.2$	$x = 0.00$	$x = 0.25$	$x = 0.50$	$x = 0.75$	$x = 1.00$
$y = 0.50$	2.8344	2.2032	2.4700	2.9856	3.8964
$y = 0.25$	1.4852	1.3606	1.7966	2.3132	3.0692
$y = 0.00$	0.0000	0.9580	1.5720	2.1220	2.8748
$z = 0.3$	$x = 0.00$	$x = 0.25$	$x = 0.50$	$x = 0.75$	$x = 1.00$
$y = 0.50$	3.2798	2.6284	2.9840	3.6728	4.8054
$y = 0.25$	1.6532	1.5636	2.1470	2.8446	3.8290
$y = 0.00$	0.0000	1.0730	1.8700	2.6080	3.5824
$z = 0.4$	$x = 0.00$	$x = 0.25$	$x = 0.50$	$x = 0.75$	$x = 1.00$
$y = 0.50$	3.5626	2.9042	1.3486	4.1766	5.4778
$y = 0.25$	1.7498	1.6916	2.3890	3.2326	4.3980
$y = 0.00$	0.0000	1.1416	2.0740	2.9620	4.1130
$z = 0.5$	$x = 0.00$	$x = 0.25$	$x = 0.50$	$x = 0.75$	$x = 1.00$
$y = 0.50$	3.7560	3.1010	3.6194	4.5616	5.9976
$y = 0.25$	1.8114	1.7800	2.5662	3.5288	4.8408
$y = 0.00$	0.0000	1.1874	2.2200	3.2320	4.5270

Table 3. 1.0 cm by 2.0 cm.

z = 0.1	0.00	0.25	0.50	0.75	1.00	1.25	1.50	1.75	2.00
y = 0.50	2.032	1.515	1.651	1.873	2.153	2.413	2.714	3.032	3.740
y = 0.25	1.111	0.985	1.225	1.483	1.756	2.032	2.312	2.611	3.102
y = 0.00	0.000	0.761	1.126	1.420	1.710	1.975	2.261	2.532	3.017
z = 0.2	0.00	0.25	0.50	0.75	1.00	1.25	1.50	1.75	2.00
y = 0.50	2.816	2.181	2.427	2.837	3.327	3.812	4.344	4.922	5.971
y = 0.25	1.457	1.349	1.776	2.249	2.742	3.241	3.749	4.287	5.086
y = 0.00	0.000	0.995	1.615	2.141	2.651	3.144	3.652	4.155	4.933
z = 0.3	0.00	0.25	0.50	0.75	1.00	1.25	1.50	1.75	2.00
y = 0.50	3.259	2.586	2.929	3.492	4.158	4.829	5.556	6.345	7.634
y = 0.25	1.624	1.549	2.122	2.768	3.446	4.129	4.828	5.565	6.599
y = 0.00	0.000	1.112	1.913	2.623	3.320	4.000	4.697	5.394	6.401
z = 0.4	0.00	0.25	0.50	0.75	1.00	1.25	1.50	1.75	2.00
y = 0.50	3.540	2.858	3.285	3.974	4.786	5.615	6.508	7.473	8.951
y = 0.25	1.720	1.676	2.361	3.148	3.975	4.820	5.682	6.588	7.813
y = 0.00	0.000	1.182	2.115	2.974	3.826	4.666	5.524	6.387	7.582
z = 0.5	0.00	0.25	0.50	0.75	1.00	1.25	1.50	1.75	2.00
y = 0.50	3.731	3.052	3.549	4.343	5.280	6.243	7.279	8.394	10.028
y = 0.25	1.782	1.763	2.536	3.438	4.393	5.374	6.377	7.428	8.813
y = 0.00	0.000	1.228	2.261	3.241	4.223	5.199	6.198	7.205	8.558

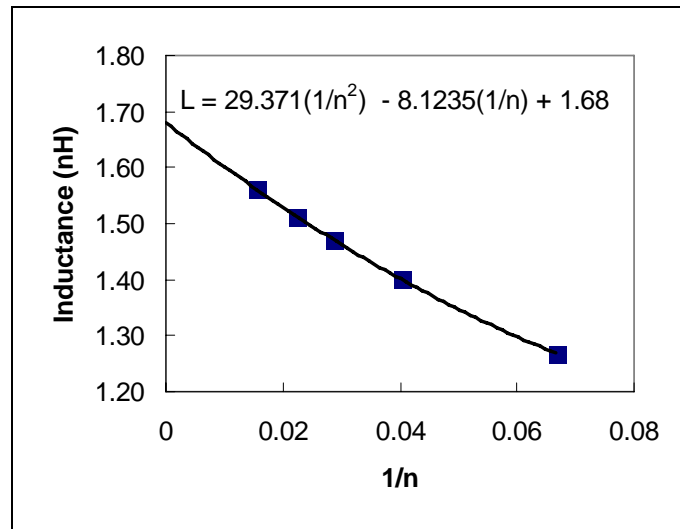


Figure 8. Convergence as a function of the inverse number of grid points.

Each table is the inductance in nanohenries for plates with various aspect ratios where one side is always 1.0 cm. The spacing between the plates is in centimeters. The inductance scales directly with the scaling of the plates. Thus, the inductance of 100-cm by 100-cm plates that are separated by 10 cm (a scaling factor of 100) gives an inductance of 108.6 nH when the hit position is in the middle (0.50 cm, 0.0 cm), with the coordinates shown in figure 2. Not included

in the tables is the fact that the inductance of any set of plates is zero when their separation distance is zero. With this fact and the use of interpolation, it is possible to estimate the inductance for any plate spacing spanned by the tables.

Now consider a design example. Assume that a 1.0-m by 2.0-m area is to be protected by EMA and the spacing between the plates is 0.1 m. One option is to use two 1.0-m by 2.0-m plates and have the current feeds at the mid-points of the 1.0-m edge. Thus, table 3 is to be used with a scale factor of 100. The hit location with the highest inductance is always at the farthest point from the current feeds,  $x = 2.0$  cm  $y = 0.5$  cm, and  $z = 0.1$  cm in table 3. Multiplying the inductance from table 3 (3.7 nH) by the scale factor gives a plate inductance of 370 nH. This inductance can be reduced by the use of two sets of parallel plates that are 1.0 m by 1.0 m, each with its own current feeds. Thus, table 2 is now to be used with a scale factor of 100. Again, using the farthest point,  $x = 1.0$  cm,  $y = 0.5$  cm, and  $z = 0.1$  cm, for the maximum inductance (2.5 nH), the maximum plate inductance is reduced to 250 nH. This reduction of the inductance must be weighed against the fact that another current feed must be added to the system. A final option is to again use 1.0-m by 2.0-m plates but have the current feed at the mid-point of the 2.0-m edge. This gives the aspect ratio of 0.5 for the plates (table 1) and a scale factor of 200. The location of the maximum inductance would then be when  $x = 0.5$  cm and  $y = 0.5$  cm but with  $z = 0.05$  cm for the spacing, which is not tabulated. Using the fact that the plate inductance is zero when  $z = 0.0$  cm and observing that the inductance increases roughly as the square root of  $z$  when  $z$  is near zero, the inductance for  $z = 0.05$  cm is approximately 0.707 times 2.251 nH, the inductance for  $z = 0.1$  cm, for an estimated value of 1.59 nH. The calculated inductance for this spacing is 1.47 nH, which shows that this interpolation gives a reasonable estimate. This gives the estimated maximum inductance for this option as 318 nH, while the calculated maximum inductance is 294 nH.

---

## 5. Conclusion

---

A procedure to estimate the inductance of two parallel plates that have a current distribution on them has been presented. Because the equations used in this procedure are long and complicated, tables of inductances for a set of parallel plates are presented. By interpolating the inductances in these tables and using a scaling law, it is possible to estimate the inductance of any set of parallel plates to within about 10%, which is a sufficient tolerance for most cases. These equations could be extended to find the inductance of more complicated structures, but they may become even more complicated.

---

## 6. References

---

1. Walker, E. H. *Defeat of Shaped Charge Devices by Active Armor*; BRL-MR-2309; U. S. Army Ballistic Research Laboratory: Aberdeen Proving Ground, MD, 1973.
2. Powell, J. D.; Littlefield, D. L. *Effect of Electromagnetic Fields on the Stability of a Perfectly Conducting, Axisymmetric Shaped-Charge Jet*; BRL-TR-3108; U. S. Army Ballistic Research Laboratory: Aberdeen Proving Ground, MD, 1990.
3. Johnson, R. F.; Toepfer, A. F. *Disruption of Shaped Charge Jets Using MHD Forces*. Final Report from Physics International to FMC, Minneapolis, MN, February 1985.
4. Shvetsov, G. A.; Matrosov, S. V.; Federov, A. B.; Babkin; Ladov, S. V. *Quest of Possibility for Controlling the Shaped Charge Effect by Electromagnetic Actions*, 4th International All-Electric Combat Vehicle Conference, Noordwijkerhout, The Netherlands, 2001.

INTENTIONALLY LEFT BLANK



---

## Appendix A. Integrals for the Inductance Calculation

---

The integration of equation 1 for the energy stored in the magnetic field starts when the expression for the magnetic vector potential in equations 11 and 12 is found. Since equations 11 and 12 become identical when the  $x$  and  $y$  subscripts of the coefficients were dropped and when the limits of integration are ignored, only equation 11 is integrated here with its  $x$  subscripts dropped.

$$A(x, y, z) = \frac{\mu_o}{4\pi} \int_{-a'}^{a'} dx' \int_{-b'}^{b'} dy' \frac{\alpha' + \beta'x' + \gamma'y' + \delta'x'y'}{\sqrt{(x-x')^2 + (y-y')^2 + z^2}} . \quad (1-A)$$

As a reminder, the rectangle is on the  $x$ - $y$  plane with its center at the origin of the coordinate system. The normal vector of the rectangle is in the positive  $z$  direction. The rectangle is oriented with one set of its parallel sides perpendicular to the  $x$ -axis. The half length of the rectangle along the  $x'$  axis is  $a'$ , and the half width of the rectangle along the  $y$  axis is  $b'$ . The integration starts when the variables are changed to  $x' = x - u$  and  $y' = y - v$ . After these new variables are substituted into the equation and after the like powers of  $u$  and  $v$  are collected in the numerator of the integrand, the equation becomes

$$\begin{aligned} A(x, y, z) = & \frac{\mu_o(\alpha' + \beta'x + \gamma'y + \delta'xy)}{4\pi} \int_{x+a'}^{x-a'} du \int_{y+b'}^{y-b'} dv \frac{1}{\sqrt{u^2 + v^2 + z^2}} \\ & - \frac{\mu_o(\beta' + \delta'y)}{4\pi} \int_{x+a'}^{x-a'} du \int_{y+b'}^{y-b'} dv \frac{u}{\sqrt{u^2 + v^2 + z^2}} \\ & - \frac{\mu_o(\gamma' + \delta'x)}{4\pi} \int_{x+a'}^{x-a'} du \int_{y+b'}^{y-b'} dv \frac{v}{\sqrt{u^2 + v^2 + z^2}} \\ & + \frac{\mu_o \delta'}{4\pi} \int_{x+a'}^{x-a'} du \int_{y+b'}^{y-b'} dv \frac{uv}{\sqrt{u^2 + v^2 + z^2}} . \end{aligned} \quad (2-A)$$

The four double integrals can be written in a general form:

$$I_{i,j}(u, v, z) = \int du \int dv \frac{u^i v^j}{\sqrt{u^2 + v^2 + z^2}} , \quad (3-A)$$

in which the subscripts  $i$  and  $j$  are the powers of  $u$  and  $v$ , respectively.

Letting  $r = \sqrt{u^2 + v^2 + z^2}$ , the expression for the integrals used in equation 2-A is

$$I_{0,0}(u, v, z) = \int du \int dv \frac{1}{\sqrt{u^2 + v^2 + z^2}} = u \ln(v+r) + v \ln(u+r) - z \arctan\left(\frac{uv}{zr}\right),$$

$$I_{1,0}(u, v, z) = \int du \int dv \frac{u}{\sqrt{u^2 + v^2 + z^2}} = \frac{vr + (u^2 + z^2) \ln(v+r)}{2},$$

$$I_{0,1}(u, v, z) = \int du \int dv \frac{v}{\sqrt{u^2 + v^2 + z^2}} = \frac{ur + (v^2 + z^2) \ln(u+r)}{2}$$

and 
$$I_{1,1}(u, v, z) = \int du \int dv \frac{uv}{\sqrt{u^2 + v^2 + z^2}} = \frac{r^3}{3}.$$

With these definitions of the integrals, equation 2-A can be written as

$$\begin{aligned} A(x, y, z) = & \frac{\mu_o(\alpha' + \beta'x + \gamma'y + \delta'xy)}{4\pi} [I_{0,0}(u, v, z)]_{x+a', y+b'}^{x-a', y-b'} \\ & - \frac{\mu_o(\beta' + \delta'y)}{4\pi} [I_{1,0}(u, v, z)]_{x+a', y+b'}^{x-a', y-b'} \\ & - \frac{\mu_o(\gamma' + \delta'x)}{4\pi} [I_{0,1}(u, v, z)]_{x+a', y+b'}^{x-a', y-b'} \\ & + \frac{\mu_o \delta'}{4\pi} [I_{1,1}(u, v, z)]_{x+a', y+b'}^{x-a', y-b'}. \end{aligned} \quad (4-A)$$

The brackets mean that the expression inside is evaluated at the limits of integration. Normal notation would have only one number in the superscript and one number in the subscript, but here there are two. In this case, the brackets mean the following:

$$[F(u, v, z)]_{x+a', y+b'}^{x-a', y-b'} = F(x-a', y-b', z) - F(x+a', y-b', z) - F(x-a', y+b', z) + F(x+a', y+b', z). \quad (5-A)$$

Note that

$$[F(u, v, z)]_{x+a', y+b'}^{x-a', y-b'} = [F(u, v, z)]_{x-a', y-b'}^{x+a', y+b'} = -[F(u, v, z)]_{x+a', y-b'}^{x-a', y+b'} = -[F(u, v, z)]_{x-a', y+b'}^{x+a', y-b'}.$$

Because of round-off error, equation 4-A should be used with caution when we are calculating the magnetic vector potential at a field point  $(x, y, z)$  far from the rectangle. The source of this round-off error comes from the subtracted terms in the definition of the brackets equation 5-A such as  $F(x-a', y-b', z) - F(x+a', y-b', z)$ , which means that the function  $I_{l,l}(u, v, z)$ , as an example, is to be evaluated at points  $(x-a', y-b', z)$  and  $(x+a', y-b', z)$  and then subtracted, that is,  $I_{l,l}(x-a', y-b', z) - I_{l,l}(x+a', y-b', z)$ . Unfortunately, the value for  $I_{l,l}(x-a', y-b', z)$  is large and nearly equal to  $I_{l,l}(x+a', y-b', z)$  at field points far from the rectangle. Subtracting two very large numbers that are nearly equal is a well-known source of round-off error in computers. Fortunately for the far field points, the magnetic vector potential can be accurately calculated with the use of its multipole expansion which does not suffer from round-off error.

To find the energy stored in the magnetic field, equation 4-A is multiplied by the current distribution in the second plate,  $J(x, y) = \alpha + \beta x + \gamma y + \delta xy$ , and integrated over the region of the second plate. The center of the second plate is located at the point  $(x_o, y_o, z)$  and has a half length  $a$  and a half height  $b$ . This multiplication would result in an awkward expression. To avoid this awkward expression, the multiplication and integration of each term in the above function  $J(x, y)$  are performed separately. Thus let

$$W_{0,0}(x_o, y_o, z) = \frac{\alpha}{2} \int_{x_o-a}^{x_o+a} dx \int_{y_o-b}^{y_o+b} dy A(x, y, z),$$

$$W_{1,0}(x_o, y_o, z) = \frac{\beta}{2} \int_{x_o-a}^{x_o+a} dx \int_{y_o-b}^{y_o+b} dy x A(x, y, z),$$

$$W_{0,1}(x_o, y_o, z) = \frac{\gamma}{2} \int_{x_o-a}^{x_o+a} dx \int_{y_o-b}^{y_o+b} dy y A(x, y, z),$$

and  $W_{1,1}(x_o, y_o, z) = \frac{\delta}{2} \int_{x_o-a}^{x_o+a} dx \int_{y_o-b}^{y_o+b} dy xy A(x, y, z).$

The integration of  $W_{1,0}(x_o, y_o, z)$  is given in detail, which starts with the substitution of equation 2-A into the above integral for  $W_{1,0}(x_o, y_o, z)$ , but only the final results for the rest are presented.

$$\begin{aligned}
W_{1,0}(x_o, y_o, z) &= \frac{\mu_o \beta}{8\pi} \int_{x_o-a}^{x_o+a} dx \int_{y_o-b}^{y_o+b} dy x (\alpha' + \beta' x + \gamma' y + \delta' xy) [I_{0,0}(u, v, z)]_{x+a', y+b'}^{x-a', y-b'} \\
&\quad - \frac{\mu_o \beta}{8\pi} \int_{x_o-a}^{x_o+a} dx \int_{y_o-b}^{y_o+b} dy x (\beta' + \delta' y) [I_{1,0}(u, v, z)]_{x+a', y+b'}^{x-a', y-b'} \\
&\quad - \frac{\mu_o \beta}{8\pi} \int_{x_o-a}^{x_o+a} dx \int_{y_o-b}^{y_o+b} dy x (\gamma' + \delta' x) [I_{0,1}(u, v, z)]_{x+a', y+b'}^{x-a', y-b'} \\
&\quad + \frac{\mu_o \beta \delta'}{8\pi} \int_{x_o-a}^{x_o+a} dx \int_{y_o-b}^{y_o+b} dy x [I_{1,1}(u, v, z)]_{x+a', y+b'}^{x-a', y-b'}
\end{aligned} \tag{6-A}$$

All the double integrals could be written in a short form as

$$S_{i,j}^{n,m} = \int_{x_o-a}^{x_o+a} dx \int_{y_o-b}^{y_o+b} dy x^n y^m [I_{i,j}(u, v, z)]_{x+a', y+b'}^{x-a', y-b'} \tag{7-A}$$

where the superscripts  $n$  and  $m$  are the powers of  $x$  and  $y$ , respectively, and the subscripts are the subscripts of the double integral defined by equation 3-A. With this notation,

$$W_{0,0}(x_o, y_o, z) = \frac{\mu_o \alpha}{8\pi} (\alpha' S_{0,0}^{0,0} + \beta' S_{0,0}^{1,0} + \gamma' S_{0,0}^{0,1} + \delta' S_{0,0}^{1,1})$$

$$- \frac{\mu_o \alpha}{8\pi} (\beta' S_{1,0}^{0,0} + \delta' S_{1,0}^{0,1} + \gamma' S_{0,1}^{0,0} + \delta' S_{0,1}^{1,0} - \delta' S_{1,1}^{0,0})$$
(8-A)

$$W_{1,0}(x_o, y_o, z) = \frac{\mu_o \beta}{8\pi} (\alpha' S_{0,0}^{1,0} + \beta' S_{0,0}^{2,0} + \gamma' S_{0,0}^{1,1} + \delta' S_{0,0}^{2,1})$$

$$- \frac{\mu_o \beta}{8\pi} (\beta' S_{1,0}^{1,0} + \delta' S_{1,0}^{1,1} + \gamma' S_{0,1}^{1,0} + \delta' S_{0,1}^{2,0} - \delta' S_{1,1}^{1,0})$$
(9-A)

$$W_{0,1}(x_o, y_o, z) = \frac{\mu_o \gamma}{8\pi} (\alpha' S_{0,0}^{0,1} + \beta' S_{0,0}^{1,1} + \gamma' S_{0,0}^{0,2} + \delta' S_{0,0}^{1,2})$$

$$- \frac{\mu_o \gamma}{8\pi} (\beta' S_{1,0}^{0,1} + \delta' S_{1,0}^{0,2} + \gamma' S_{0,1}^{0,1} + \delta' S_{0,1}^{1,1} - \delta' S_{1,1}^{0,1})$$
(10-A)

and

$$W_{1,1}(x_o, y_o, z) = \frac{\mu_o \delta}{8\pi} (\alpha' S_{0,0}^{1,1} + \beta' S_{0,0}^{2,1} + \gamma' S_{0,0}^{1,2} + \delta' S_{0,0}^{2,2})$$

$$- \frac{\mu_o \delta}{8\pi} (\beta' S_{1,0}^{1,1} + \delta' S_{1,0}^{1,2} + \gamma' S_{0,1}^{1,1} + \delta' S_{0,1}^{2,1} - \delta' S_{1,1}^{1,1})$$
(11-A)

Thus, there are a total of 24 different double integrals to be evaluated. The procedure for evaluating all these double integrals starts with the removal of the bracket notation in equation 7-A and the terms written explicitly.

$$S_{i,j}^{n,m} = \int_{x_o-a}^{x_o+a} dx \int_{y_o-b}^{y_o+b} dy x^n y^m I_{i,j}(x-a', y-b', z)$$

$$- \int_{x_o-a}^{x_o+a} dx \int_{y_o-b}^{y_o+b} dy x^n y^m I_{i,j}(x+a', y-b', z)$$

$$- \int_{x_o-a}^{x_o+a} dx \int_{y_o-b}^{y_o+b} dy x^n y^m I_{i,j}(x-a', y+b', z)$$

$$+ \int_{x_o-a}^{x_o+a} dx \int_{y_o-b}^{y_o+b} dy x^n y^m I_{i,j}(x+a', y+b', z).$$

The next step is to change the variables in each term:

$$S_{i,j}^{n,m} = \int_{x_o-a-a'}^{x_o+a-a'} dp \int_{y_o-b-b'}^{y_o+b-b'} dq (p+a')^n (q+b')^m I_{i,j}(p, q, z)$$

$$\begin{aligned}
& - \int_{x_o-a+a'}^{x_o+a+a'} dp \int_{y_o-b-b'}^{y_o+b-b'} dq (p-a')^n (q+b')^m I_{i,j}(p,q,z) \\
& - \int_{x_o-a-a'}^{x_o+a-a'} dp \int_{y_o-b+b'}^{y_o+b+b'} dq (p+a')^n (q-b')^m I_{i,j}(p,q,z) \\
& + \int_{x_o-a+a'}^{x_o+a+a'} dp \int_{y_o-b+b'}^{y_o+b+b'} dq (p-a')^n (q-b')^m I_{i,j}(p,q,z) .
\end{aligned} \tag{12-A}$$

The term in front of each  $I_{i,j}(p,q,z)$  can be multiplied into a sum of terms such as

$$(p+a')^n (q+b')^m = \sum_{k=0, l=0}^{k=n, l=m} C_{k,l} p^k q^l . \text{ Thus the double integrals in equation 12-A now have the form}$$

$$H_{i,j}^{k,l} = \int dp \int dq p^k q^l I_{i,j}(p,q,z) \tag{13-A}$$

whose expressions can now be determined. With the notation defined by equation 13-A, the integral  $S_{i,j}^{2,0}$  is given as an example. Thus,

$$\begin{aligned}
S_{i,j}^{2,0} &= \int_{x_o-a-a'}^{x_o+a-a'} dp \int_{y_o-b-b'}^{y_o+b-b'} dq (p^2 + 2a'p + (a')^2) I_{i,j}(p,q,z) \\
& - \int_{x_o-a+a'}^{x_o+a+a'} dp \int_{y_o-b-b'}^{y_o+b-b'} dq (p^2 - 2a'p + (a')^2) I_{i,j}(p,q,z) \\
& - \int_{x_o-a-a'}^{x_o+a-a'} dp \int_{y_o-b+b'}^{y_o+b+b'} dq (p^2 + 2a'p + (a')^2) I_{i,j}(p,q,z) \\
& + \int_{x_o-a+a'}^{x_o+a+a'} dp \int_{y_o-b+b'}^{y_o+b+b'} dq (p^2 - 2a'p + (a')^2) I_{i,j}(p,q,z) .
\end{aligned}$$

After the definition for bracketed terms and the definition for the double integrals are used, equation 11-A, this expression becomes

$$\begin{aligned}
S_{i,j}^{2,0} &= \left[ H_{i,j}^{2,0} + 2a'H_{i,j}^{1,0} + (a')^2 H_{i,j}^{0,0} \right]_{x_o-a-a', y_o-b-b'}^{x_o+a-a', y_o+b-b'} - \left[ H_{i,j}^{2,0} - 2a'H_{i,j}^{1,0} + (a')^2 H_{i,j}^{0,0} \right]_{x_o-a+a', y_o-b-b'}^{x_o+a+a', y_o+b-b'} \\
& - \left[ H_{i,j}^{2,0} + 2a'H_{i,j}^{1,0} + (a')^2 H_{i,j}^{0,0} \right]_{x_o-a-a', y_o-b+b'}^{x_o+a-a', y_o+b+b'} + \left[ H_{i,j}^{2,0} - 2a'H_{i,j}^{1,0} + (a')^2 H_{i,j}^{0,0} \right]_{x_o-a+a', y_o-b+b'}^{x_o+a+a', y_o+b+b'} , \tag{14-A}
\end{aligned}$$

where the functions  $H_{i,j}^{n,m}(p, q, z)$  were abbreviated to  $H_{i,j}^{n,m}$ . Note that equation 12-A holds for any values for  $i$  and  $j$ . Thus there are a total of nine unique forms for  $S_{i,j}^{n,m}$  in equations 6-A through 9-A. The other eight forms are

$$\begin{aligned}
S_{i,j}^{0,0} &= \left[ H_{i,j}^{0,0} \right]_{x_o-a-a', y_o-b-b'}^{x_o+a-a', y_o+b-b'} - \left[ H_{i,j}^{0,0} \right]_{x_o-a+a', y_o-b-b'}^{x_o+a+a', y_o+b-b'} - \left[ H_{i,j}^{0,0} \right]_{x_o-a-a', y_o-b+b'}^{x_o+a-a', y_o+b+b'} + \left[ H_{i,j}^{0,0} \right]_{x_o-a+a', y_o-b+b'}^{x_o+a+a', y_o+b+b'} \\
S_{i,j}^{1,0} &= \left[ H_{i,j}^{1,0} + a'H_{i,j}^{0,0} \right]_{x_o-a-a', y_o-b-b'}^{x_o+a-a', y_o+b-b'} - \left[ H_{i,j}^{1,0} - a'H_{i,j}^{0,0} \right]_{x_o-a+a', y_o-b-b'}^{x_o+a+a', y_o+b-b'} \\
&\quad - \left[ H_{i,j}^{1,0} - a'H_{i,j}^{0,0} \right]_{x_o-a-a', y_o-b+b'}^{x_o+a-a', y_o+b+b'} + \left[ H_{i,j}^{1,0} + a'H_{i,j}^{0,0} \right]_{x_o-a+a', y_o-b+b'}^{x_o+a+a', y_o+b+b'} \\
S_{i,j}^{0,1} &= \left[ H_{i,j}^{0,1} + b'H_{i,j}^{0,0} \right]_{x_o-a-a', y_o-b-b'}^{x_o+a-a', y_o+b-b'} - \left[ H_{i,j}^{0,1} + b'H_{i,j}^{0,0} \right]_{x_o-a+a', y_o-b-b'}^{x_o+a+a', y_o+b-b'} \\
&\quad - \left[ H_{i,j}^{0,1} - b'H_{i,j}^{0,0} \right]_{x_o-a-a', y_o-b+b'}^{x_o+a-a', y_o+b+b'} + \left[ H_{i,j}^{0,1} + b'H_{i,j}^{0,0} \right]_{x_o-a+a', y_o-b+b'}^{x_o+a-a', y_o+b+b'} \\
S_{i,j}^{1,1} &= \left[ H_{i,j}^{1,1} + a'H_{i,j}^{0,1} + b'H_{i,j}^{1,0} + a'b'H_{i,j}^{0,0} \right]_{x_o-a-a', y_o-b-b'}^{x_o+a-a', y_o+b-b'} \\
&\quad - \left[ H_{i,j}^{1,1} - a'H_{i,j}^{0,1} + b'H_{i,j}^{1,0} - a'b'H_{i,j}^{0,0} \right]_{x_o-a+a', y_o-b-b'}^{x_o+a+a', y_o+b-b'} \\
&\quad - \left[ H_{i,j}^{1,1} + a'H_{i,j}^{0,1} - b'H_{i,j}^{1,0} - a'b'H_{i,j}^{0,0} \right]_{x_o-a-a', y_o-b+b'}^{x_o+a-a', y_o+b+b'} \\
&\quad + \left[ H_{i,j}^{1,1} - a'H_{i,j}^{0,1} - b'H_{i,j}^{1,0} + a'b'H_{i,j}^{0,0} \right]_{x_o-a+a', y_o-b+b'}^{x_o+a-a', y_o+b+b'} \\
S_{i,j}^{2,1} &= \left[ H_{i,j}^{2,1} + 2a'H_{i,j}^{1,1} + (a')^2 H_{i,j}^{0,1} + b'H_{i,j}^{2,0} + 2a'b'H_{i,j}^{1,0} + (a')^2 H_{i,j}^{0,0} \right]_{x_o-a-a', y_o-b-b'}^{x_o+a-a', y_o+b-b'} \\
&\quad - \left[ H_{i,j}^{2,1} - 2a'H_{i,j}^{1,1} + (a')^2 H_{i,j}^{0,1} + b'H_{i,j}^{2,0} - 2a'b'H_{i,j}^{1,0} + (a')^2 H_{i,j}^{0,0} \right]_{x_o-a+a', y_o-b-b'}^{x_o+a+a', y_o+b-b'} \\
&\quad - \left[ H_{i,j}^{2,1} + 2a'H_{i,j}^{1,1} + (a')^2 H_{i,j}^{0,1} - b'H_{i,j}^{2,0} - 2a'b'H_{i,j}^{1,0} + (a')^2 H_{i,j}^{0,0} \right]_{x_o-a-a', y_o-b+b'}^{x_o+a-a', y_o+b+b'} \\
&\quad + \left[ H_{i,j}^{2,1} - 2a'H_{i,j}^{1,1} + (a')^2 H_{i,j}^{0,1} - b'H_{i,j}^{2,0} + 2a'b'H_{i,j}^{1,0} + (a')^2 H_{i,j}^{0,0} \right]_{x_o-a+a', y_o-b+b'}^{x_o+a+a', y_o+b+b'} \\
S_{i,j}^{0,2} &= \left[ H_{i,j}^{0,2} + 2b'H_{i,j}^{0,1} + (b')^2 H_{i,j}^{0,0} \right]_{x_o-a-a', y_o-b-b'}^{x_o+a-a', y_o+b-b'} - \left[ H_{i,j}^{0,2} + 2b'H_{i,j}^{0,1} + (b')^2 H_{i,j}^{0,0} \right]_{x_o-a+a', y_o-b-b'}^{x_o+a+a', y_o+b-b'} \\
&\quad - \left[ H_{i,j}^{0,2} - 2b'H_{i,j}^{0,1} + (b')^2 H_{i,j}^{0,0} \right]_{x_o-a-a', y_o-b+b'}^{x_o+a-a', y_o+b+b'} + \left[ H_{i,j}^{0,2} - 2b'H_{i,j}^{0,1} + (b')^2 H_{i,j}^{0,0} \right]_{x_o-a+a', y_o-b+b'}^{x_o+a+a', y_o+b+b'} \\
S_{i,j}^{1,2} &= \left[ H_{i,j}^{1,2} + 2b'H_{i,j}^{1,1} + (b')^2 H_{i,j}^{1,0} + a'H_{i,j}^{0,2} + 2a'b'H_{i,j}^{0,1} + (b')^2 H_{i,j}^{0,0} \right]_{x_o-a-a', y_o-b-b'}^{x_o+a-a', y_o+b-b'} \\
&\quad - \left[ H_{i,j}^{1,2} + 2b'H_{i,j}^{1,1} + (b')^2 H_{i,j}^{1,0} - a'H_{i,j}^{0,2} - 2a'b'H_{i,j}^{0,1} + (b')^2 H_{i,j}^{0,0} \right]_{x_o-a+a', y_o-b-b'}^{x_o+a+a', y_o+b-b'} \\
&\quad - \left[ H_{i,j}^{1,2} - 2b'H_{i,j}^{1,1} + (b')^2 H_{i,j}^{1,0} + a'H_{i,j}^{0,2} - 2a'b'H_{i,j}^{0,1} + (b')^2 H_{i,j}^{0,0} \right]_{x_o-a-a', y_o-b+b'}^{x_o+a-a', y_o+b+b'} \\
&\quad + \left[ H_{i,j}^{1,2} - 2b'H_{i,j}^{1,1} + (b')^2 H_{i,j}^{1,0} - a'H_{i,j}^{0,2} + 2a'b'H_{i,j}^{0,1} + (b')^2 H_{i,j}^{0,0} \right]_{x_o-a+a', y_o-b+b'}^{x_o+a-a', y_o+b+b'} \\
S_{i,j}^{2,2} &= \left[ \begin{aligned} &H_{i,j}^{2,2} + 2a'H_{i,j}^{1,2} + (a')^2 H_{i,j}^{0,2} + 2b'H_{i,j}^{2,1} + 4a'b'H_{i,j}^{1,1} + \\ &2(a')^2 b'H_{i,j}^{0,1} + (b')^2 H_{i,j}^{2,0} + 2a'(b')^2 H_{i,j}^{1,0} + (a'b')^2 H_{i,j}^{0,0} \end{aligned} \right]_{x_o-a-a', y_o-b-b'}^{x_o+a-a', y_o+b-b'} \\
&\quad - \left[ \begin{aligned} &H_{i,j}^{2,2} - 2a'H_{i,j}^{1,2} + (a')^2 H_{i,j}^{0,2} + 2b'H_{i,j}^{2,1} - 4a'b'H_{i,j}^{1,1} + \\ &2(a')^2 b'H_{i,j}^{0,1} + (b')^2 H_{i,j}^{2,0} - 2a'(b')^2 H_{i,j}^{1,0} + (a'b')^2 H_{i,j}^{0,0} \end{aligned} \right]_{x_o-a+a', y_o-b-b'}^{x_o+a+a', y_o+b-b'}
\end{aligned}$$

$$\begin{aligned}
& - \left[ \begin{array}{l} H_{i,j}^{2,2} + 2a'H_{i,j}^{1,2} + (a')^2 H_{i,j}^{0,2} - 2b'H_{i,j}^{2,1} - 4a'b'H_{i,j}^{1,1} - \\ 2(a')^2 b'H_{i,j}^{0,1} + (b')^2 H_{i,j}^{2,0} + 2a'(b')^2 H_{i,j}^{1,0} + (a'b')^2 H_{i,j}^{0,0} \end{array} \right]_{x_o - a - a', y_o - b + b'}^{x_o + a - a', y_o + b + b'} \\
& + \left[ \begin{array}{l} H_{i,j}^{2,2} - 2a'H_{i,j}^{1,2} + (a')^2 H_{i,j}^{0,2} - 2b'H_{i,j}^{2,1} + 4a'b'H_{i,j}^{1,1} - \\ 2(a')^2 b'H_{i,j}^{0,1} + (b')^2 H_{i,j}^{2,0} - 2a'(b')^2 H_{i,j}^{1,0} + (a'b')^2 H_{i,j}^{0,0} \end{array} \right]_{x_o - a + a', y_o - b + b'}^{x_o + a + a', y_o + b + b'}
\end{aligned}$$

These forms or expressions for  $S_{i,j}^{n,m}$  are substituted into equations 6-A through 9-A with the appropriate values for the indexes. After this substitution, there are a number of  $H_{i,j}^{k,l}$  that appear more than once. After we take into account the duplicate integrals, there are 25 unique  $H_{i,j}^{k,l}$ , which are given below where  $r = \sqrt{p^2 + q^2 + z^2}$ .

$$H_{0,0}^{0,0} = \frac{r}{6}(2z^2 - p^2 - q^2) + \frac{q}{2}(p^2 - z^2)\ln(q+r) + \frac{u}{2}(q^2 - z^2)\ln(p+r) - pqz \arctan\left(\frac{pq}{rz}\right)$$

$$H_{0,0}^{1,0} = \frac{pr}{48}(3z^2 - q^2 - 6p^2) + \frac{p^3q}{3}\ln(q+r)$$

$$+ \frac{1}{48}(6q^2z^2 - 3z^4 - 12p^2z^2 + q^4 + 12p^2q^2)\ln(p+r) - \frac{zq}{6}(z^2 + 3p^2)\arctan\left(\frac{pq}{rz}\right)$$

$$H_{0,0}^{0,1} = \frac{qr}{48}(3z^2 - p^2 - 6q^2) + \frac{1}{48}(6p^2z^2 - 3z^4 - 12q^2z^2 + p^4 + 12p^2q^2)\ln(q+r)$$

$$+ \frac{pq^3}{3}\ln(p+r) - \frac{zp}{6}(z^2 + 3q^2)\arctan\left(\frac{pq}{rz}\right)$$

$$H_{0,0}^{1,1} = \frac{pqr}{60}(z^2 - p^2 - q^2) + \frac{p^3}{60}(5z^2 + p^2 + 10q^2)\ln(q+r) + \frac{v^3}{60}(5z^2 + 10p^2 + q^2)\ln(p+r)$$

$$- \frac{z}{60}(z^4 + 5p^2z^2 + 5q^2z^2 + 15p^2q^2)\arctan\left(\frac{pq}{rz}\right)$$

$$H_{0,1}^{0,0} = \frac{rq}{24}(3p^2 - 2q^2 - 5z^2) + \frac{1}{24}(6p^2z^2 + p^4 - 3z^2)\ln(q+r)$$

$$+ \frac{pq}{6}(3z^2 + q^2)\ln(p+r) - \frac{pz^3}{3}\arctan\left(\frac{pq}{rz}\right)$$

$$H_{0,1}^{1,0} = \frac{pq}{240}(22p^2 - 3q^2 - 7z^2) + \frac{p^3}{30}(5z^2 + p^2)\ln(q+r)$$

$$+ \frac{q}{240}(15z^4 + 10q^2z^2 + 60p^2z^2 + 3q^4 + 20p^2q^2)\ln(p+r) - \frac{z^3}{30}(z^2 + 5p^2)\arctan\left(\frac{pq}{rz}\right)$$

$$H_{0,1}^{0,1} = \frac{r}{120}(9p^2z^2 - 8z^4 - 16q^2z^2 - 8q^4 + 9p^2q^2 + 2p^4) + \frac{p}{8}(q^2 + z^2)^2\ln(p+r)$$

$$H_{0,1}^{1,1} = \frac{pr}{288}(4p^4 + 16p^2q^2 - 3q^4 + 16p^2z^2 - 6q^2z^2 - 3z^4) \\ + \frac{1}{192}(2z^6 + 6q^2z^4 + 12p^2z^4 + 6q^4z^2 + 24p^2q^2z^2 + 2q^6 + 12p^2q^4)\ln(p+r)$$

$$H_{1,0}^{0,0} = \frac{pr}{24}(3q^2 - 2p^2 - 5z^2) + \frac{pq}{6}(p^2 + 3z^2)\ln(q+r) \\ + \frac{1}{24}(q^4 + 6q^2z^2 - 3z^4)\ln(p+r) - \frac{vz^3}{3}\arctan\left(\frac{pq}{rz}\right)$$

$$H_{1,0}^{0,1} = \frac{pqr}{240}(22q^2 - 3p^2 - 7z^2) + \frac{P}{240}(15z^4 + 60q^2z^2 + 10p^2z^2 + 20p^2q^2 + 3p^4)\ln(q+r) \\ + \frac{q^3}{30}(q^2 + 5z^2)\ln(p+r) - \frac{z^3}{30}(q^2 + 5z^2)\arctan\left(\frac{pq}{rz}\right)$$

$$H_{1,0}^{1,0} = \frac{r}{120}(9q^2z^2 - 8z^4 - 16p^2z^2 + 2q^4 + 9p^2q^2 - 8p^4) + \frac{q}{8}(z^2 + u^2)^2\ln(q+r)$$

$$H_{1,0}^{1,1} = \frac{qr}{288}(4q^4 + 16p^2q^2 - 3p^4 - 3z^4 + 16q^2z^2 - 6p^2z^2) \\ + \frac{1}{96}(z^6 + 6q^2z^4 + 3p^2z^4 + 12p^2q^2z^2 + 3p^4z^2 + 6p^4q^2 + p^6)\ln(q+r)$$

$$H_{1,1}^{0,0} = \frac{pqr}{120}(18z^2 + 7q^2 + 7p^2) + \frac{P}{120}(15z^4 + 10p^2z^2 + 3p^4)\ln(q+r) \\ + \frac{q}{120}(15z^4 + 10q^2z^2 + 3q^3)\ln(p+r) - \frac{z^5}{15}\arctan\left(\frac{pq}{rz}\right)$$

$$H_{1,1}^{0,1} = \frac{pr}{720}(33z^4 + 66q^2z^2 + 26p^2z^2 + 33q^4 + 26p^2q^2 + 8p^4) + \frac{1}{48}(z^2 + q^2)^3\ln(p+r)$$

$$H_{1,1}^{1,0} = \frac{qr}{720}(33z^4 + 26q^2z^2 + 66p^2z^2 + 8q^4 + 26p^2q^2 + 33p^4) + \frac{1}{48}(z^2 + p^2)^3\ln(q+r)$$

$$H_{1,1}^{1,1} = \frac{r^7}{105}$$

$$H_{0,0}^{2,0} = \frac{r}{180}(9q^2z^2 - 8z^4 + 4p^2z^2 + 2q^4 - p^2q^2 - 18p^4) + \frac{q}{12}(z^4 + 3p^4)\ln(q+r) \\ + \frac{p^3}{6}(q^2 - z^2)\ln(p+r) - \frac{p^3qz}{3}\arctan\left(\frac{pq}{zr}\right)$$



$$\begin{aligned}
H_{0,1}^{2,0} &= \frac{qr}{3240} (99z^4 + 78q^2z^2 - 27p^2z^2 + 24q^4 - 12p^2q^2 + 234p^4) \\
&+ \frac{1}{72} (z^6 + 9p^4z^2 + 2p^6) \ln(q+r) + \frac{p^3q}{18} (3z^2 + q^2) \ln(p+r) - \frac{p^3z^3}{9} \arctan\left(\frac{pq}{zr}\right) \\
H_{0,0}^{2,1} &= \frac{qr}{432} (16q^2z^2 - 3z^4 + 3p^2z^2 + 4q^4 - 2p^2q^2 - 6p^4) \\
&+ \frac{1}{144} (z^6 + 6q^2z^4 + 9p^4z^2 + 18p^4q^2 + 2p^6) \ln(v+r) + \frac{p^3q^3}{9} \ln(p+r) \\
&- \frac{p^3z}{18} (z^2 + 3q^2) \arctan\left(\frac{pq}{zr}\right) \\
H_{0,0}^{1,2} &= \frac{pr}{432} (16p^2z^2 - 3z^4 + 3q^2z^2 + 4p^4 - 2p^2q^2 - 6q^4) + \frac{p^3q^3}{9} \ln(v+r) \\
&+ \frac{1}{144} (z^6 + 6p^2z^4 + 9q^4z^2 + 18p^2q^4 + 2q^6) \ln(u+r) - \frac{q^3z}{18} (z^2 + 3p^2) \arctan\left(\frac{pq}{zr}\right) \\
H_{0,0}^{0,2} &= \frac{r}{180} (9p^2z^2 - 8z^4 + 4q^2z^2 + 2p^4 - p^2q^2 - 18q^4) + \frac{p}{12} (z^4 + 3q^4) \ln(p+r) \\
&+ \frac{q^3}{6} (p^2 - z^2) \ln(q+r) - \frac{pq^3z}{3} \arctan\left(\frac{pq}{zr}\right) \\
H_{1,0}^{0,2} &= \frac{pr}{1080} (33z^4 + 26p^2z^2 - 9q^2z^2 + 8p^4 - 4p^2q^2 + 78q^4) + \frac{pq^3}{18} (3z^2 + p^2) \ln(q+r) \\
&+ \frac{1}{72} (z^6 + 9q^4z^2 + 2q^6) \ln(p+r) - \frac{q^3z^3}{9} \arctan\left(\frac{pq}{zr}\right) \\
H_{0,0}^{2,2} &= \frac{r}{3780} (16z^6 - 8q^2z^4 - 8p^2z^4 + 111q^4z^2 + 12p^2q^2z^2 + 111p^4z^2 + 30q^6 \\
&- 15p^2q^4 - 15p^4q^2 + 30p^6) + \frac{q^3}{36} (z^4 + 3p^4) \ln(q+r) + \frac{p^3}{36} (z^4 + 3q^4) \ln(p+r) \\
&- \frac{p^3q^3z}{9} \arctan\left(\frac{pq}{zr}\right) \\
H_{1,0}^{1,2} &= \frac{r}{2520} (16z^6 - 8q^2z^4 + 48p^2z^4 + 111q^4z^2 - 16p^2q^2z^2 + 48p^4z^2 + 30q^6 \\
&+ 111p^2q^4 - 8p^4q^2 + 16p^6) + \frac{q^3}{24} (z^2 + p^2)^2 \ln(q+r)
\end{aligned}$$

$$H_{0,1}^{2,1} = \frac{r}{2520}(16z^6 - 8p^2z^4 + 48q^2z^4 + 111p^4z^2 - 16p^2q^2z^2 + 48q^4z^2 + 30p^6 \\ + 111p^4q^2 - 8p^2q^4 + 16q^6) + \frac{p^3}{24}(z^2 + q^2)^2 \ln(p+r)$$

<u>NO. OF COPIES</u>	<u>ORGANIZATION</u>
1 (PDF ONLY)	DEFENSE TECHNICAL INFORMATION CTR DTIC OCA 8725 JOHN J KINGMAN RD STE 0944 FORT BELVOIR VA 22060-6218
1	US ARMY RSRCH DEV & ENGRG CMD SYSTEMS OF SYSTEMS INTEGRATION AMSRD SS T 6000 6TH ST STE 100 FORT BELVOIR VA 22060-5608
1	INST FOR ADVNCD TCHNLGY THE UNIV OF TEXAS AT AUSTIN 3925 W BRAKER LN STE 400 AUSTIN TX 78759-5316
1	DIRECTOR US ARMY RESEARCH LAB IMNE ALC IMS 2800 POWDER MILL RD ADELPHI MD 20783-1197
1	DIRECTOR US ARMY RESEARCH LAB AMSRD ARL CI OK TL 2800 POWDER MILL RD ADELPHI MD 20783-1197
2	DIRECTOR US ARMY RESEARCH LAB AMSRD ARL CS OK T 2800 POWDER MILL RD ADELPHI MD 20783-1197
2	DIRECTOR US ARMY RSCH LABORATORY ATTN AMSRD ARL SE DP S SCOZZIE W TIPTON 2800 POWDER MILL RD ADELPHI MD 20783-1197
2	US ARMY TARDEC ATTN AMSTA TR T FURMANIAK D TEMPLETON WARREN MI 48397-5000
1	CDR TAAC ARMNTS CMD SURVIVABILITY TECH CTR ATTN SFAE GCSS W GSI H J ROWE WARREN MI 43897-5000

<u>NO. OF COPIES</u>	<u>ORGANIZATION</u>
1	NUMEREX ATTN J LUGINSLAND 2309 RENARD PL SE STE 220 ALBUQUERQUE NM 87106-4259
1	SAIC ATTN A J TOEPFER 2109 AIR PARK RD ALBUQUERQUE NM 87106
2	SAIC ATTN MS SH 4-5 R FORD A MONDELLI 1410 SPRING HILL RD STE 400 MCCLEAN VA 22102
1	SAIC ATTN K A JAMISON PO BOX 4216 FT WALTON BEACH FL 32549
1	BATTELLE CORP ATTN M FISHER 505 KING AVE COLUMBUS OH 43201
1	ASST SECY OF THE ARMY FOR ACQUISITION LOGISTICS AND TECHNOLOGY ATTN SAAL TT M FREEMAN 2511 JEFFERSON DAVIS HWY RM 9800 ARLINGTON VA 22202-3911
1	SANDIA NATL LABORATORIES ATTN C GARASI PO BOX 5800 MAIL STOP 1186 ALBUQUERQUE NM 87185-1186
	<u>ABERDEEN PROVING GROUND</u>
1	DIRECTOR US ARMY RSCH LABORATORY ATTN AMSRD ARL CI OK (TECH LIB) BLDG 4600
1	DIRECTOR US ARMY RSCH LABORATORY ATTN AMSRD ARL WM B M ZOLTOSKI BLDG 4600
1	DIRECTOR US ARMY RSCH LABORATORY ATTN AMSRD ARL WM BC A ZIELINSKI BLDG 390

NO. OF  
COPIES ORGANIZATION

- 1 DIRECTOR  
US ARMY RSCH LABORATORY  
ATTN AMSRD ARL WM EG E SCHMIDT  
BLDG 4600
  
- 6 DIRECTOR  
US ARMY RSCH LABORATORY  
ATTN AMSRD ARL WM TA M KEELE  
P BARTKOWSKI B DONEY  
P KINGMAN A BARD J RUNYEON  
BLDG 393
  
- 1 DIRECTOR  
US ARMY RSCH LABORATORY  
ATTN AMSRD ARL WM TC W WALTERS  
BLDG 309
  
- 10 DIRECTOR  
US ARMY RSCH LABORATORY  
ATTN AMSRD ARL WM TE P BERNING  
C HUMMER (5 CYS) T KOTTKE  
A NILER J POWELL  
G THOMSON  
BLDG 120